Investigation of noise correlations in the phase-locked class-A VECSEL array

Sopfy Karuseichyk, Vishwa Pal, Sahil Sahoo, Grégoire Beaudoin, Isabelle Sagnes, Fabien Bretenaker

Research Article | Vol. 31, No. 25 / 4 Dec 2023 / Optics Express 41713
Optics EXPRESS

Investigation of noise correlations in the phase-locked class-A VECSEL array

Sopfy Karuseichyk,[1,*] Vishwa Pal,[2] Sahil Sahoo,[2] Grégoire Beaudoin,[3] Isabelle Sagnes,[3] and Fabien Bretenaker[1,4]

[1]Université Paris-Saclay, ENS, CNRS, CentraleSupélec, LuMIn, Gif-sur-Yvette, France
[2]Department of Physics, Indian Institute of Technology Ropar, Rupnagar, Punjab 140001, India
[3]C2N, CNRS, Université Paris-Saclay, Palaiseau, France
[4]Advanced Technology Development Center, Indian Institute of Technology Kharagpur, Kharagpur, West Bengal 721302, India
[*]sonya.karuseichyk@universite-paris-saclay.fr

Abstract: We theoretically and experimentally study the noise correlations in an array of lasers based on a VECSEL (Vertical External Cavity Surface Emitting Laser) architecture. The array of two or three lasers is created inside a planar degenerate cavity with a mask placed in a self-imaging position. Injection from each laser to its neighbors is created by diffraction, which creates a controllable complex coupling coefficient. The noise correlations between the different modes are observed to be dramatically different when the lasers are phase-locked or unlocked. These results are well explained by a rate equation model that takes into account the class-A dynamics of the lasers. This model permits the isolatation of the influence of the complex coupling coefficients and of the Henry α-factor on the noise behavior of the laser array.

1. Introduction

Integration of lasers into communication technologies and computational systems is growing every day. One example of such applications of lasers relies on laser arrays. Indeed, such a system of many coupled oscillators recently became a promising device to solve several types of problems. For example, utilization of the far-field emission of the laser addresses applications to beam shaping [1–3]. The observation of the laser steady-state can be used to solve complicated optimization problems by searching the global steady-state solution of the system [4–9]. Besides, it was recently demonstrated numerically that coherent laser arrays exhibit collective neural computing capabilities [10,11], where the individual lasers act as the array nodes, and the coupling strength between the lasers plays the role of the weight coefficients. Moreover, emission from such laser arrays can find applications in other extremely important areas, such as data transmission [12,13], optical memories [14–17], tweezers for atom arrays [18,19], and others.

However, it is well known that noise plays a crucial role in the dynamics of lasers [20]. In the case of the use of a laser array as an analog computing machine, the multiplicative noise (transfer of noise from pump) can greatly affect the phase-locking of lasers by reducing the number of phase-locked lasers. This will limit the scalability of the simulator, and thus the capability of solving large-scale problems. Further, noise can prevent the laser simulator from dissipating into a minimal loss (ground state) state of phase-locked lasers, thus, it will not be able to find an optimal solution of a given problem. Therefore, to improve the performance of a laser simulator, it is very important to study the role of noise in such laser arrays. Moreover, a complete characterization of such noise requires not only to measure the noise of individual lasers in the array, but also their correlations. Such correlations have, for example, already been shown to play an important role in dual-frequency lasers used in atomic clock applications [21–23], and

#501051 https://doi.org/10.1364/OE.501051
Journal © 2023 Received 19 Jul 2023; revised 29 Sep 2023; accepted 22 Oct 2023; published 28 Nov 2023

Optics EXPRESS

also to be able to reveal the dynamics of lasers, depending in particular on whether they belong to the class-A or class-B dynamical regime [24,25].

Diagnosing the behavior of an array of coupled lasers by using its intensity noise properties requires to use a relatively quiet laser. However, till now, laser array phase-locking was mainly investigated in solid-state Nd:YAG lasers [26], fiber lasers [27,28], laser diodes [29–31], and CO_2 gas lasers [32], which are usually quite noisy systems. In spite of their versatility in the context of arrays of lasers based on degenerate cavity architectures [33], Nd:YAG lasers are not the best candidates to achieve low noise operation. Indeed, they are intrinsically very noisy because they belong to the class-B dynamic class [34]. On the contrary, VECSELs (Vertical External Cavity Surface Emitting Lasers) are well known to be extremely quiet lasers, because their class-A dynamical behavior filters out the pump noise above the cavity cut-off frequency [35–37]. Besides, the external cavity operation allows to implement a degenerate cavity configuration [38]. However, one must take into consideration the fact that the semiconductor gain medium of VECSELs exhibits a non-negligible Henry α-coefficient (also called phase-amplitude coupling coefficient or linewidth enhancement factor), which tends to affect the laser phase-locking behavior [39]. Indeed, the value of this linewidth enhancement factor in different types of semiconductor gain chips typically ranges from 3 to 10 [40–43] and can even be much larger (up to 60) for shallow quantum wells chips [44]. These values are much larger than those of Nd:YAG lasers (α 0.3) [45].

The aim of this paper is thus to study noise correlations in both independent and phase-locked VECSEL laser arrays. More precisely, we aim at analyzing the influence of the phase-locking behavior on the laser intensity noise properties. The experimental implementation of the laser array is based on the division of a degenerate cavity into several independent lasers using a loss mask. The amount of coupling between the channels is controlled by the loss-mask displacement, contrary to degenerate cavity VECSEL configurations in which the mask is deposited on the gain medium [46]. The experiments performed below are also compared to the predictions of our model that takes into account the three particular aspects of our VECSEL-based laser array: i) the class-A dynamics; ii) the large α-factor, and iii) the complex nature of the coupling coefficient between the lasers induced by diffraction.

2. Experiment: phase-locking of laser array and noise

Before entering the theoretical and experimental description of the laser noise, this section aims at describing the experimental scheme, discussing the coupling mechanism between the lasers in the array, and observing the phase-locking behavior of lasers.

2.1. Experimental setup

The experimental setup is schematized in Fig. 1. The VECSEL array is based on a gain chip obtained by MOVPE in a VEECO-D180 reactor on GaAs substrate. It consists of a multi-layered semiconductor structure consisting of a distributed Bragg reflector (DBR), a gain region consisting of twelve InGaAs/GaAsP quantum wells, and an antireflection coating. Excitation of the chip is provided by optical pumping at 808 nm with 0.86 W power. Heat is extracted from the gain chip by attaching it to a Peltier cooler using thermal paste. The Peltier cooler itself is mounted with thermal glue on a copper radiator, in which cooling water is circulated. The Peltier temperature is maintained at 20°C. Heat dissipation plays a significant role in preventing structure deformation and efficiency rollover [47]. In our case, since no particular heat treatment method is applied to the gain chip [47], the thermal profile induces a positive lens that dominates over the negative electronic lens [48].

The cavity is closed by a planar output coupler with a 0.8% transmission at the $\lambda = 1.06\,\mu$m laser wavelength. Spatial degeneracy and stability of the cavity are provided by an intracavity telescope in 4f-configuration. Two positive lenses (focal lengths $f_1 = 5$ cm and $f_2 = 20$ cm)

Optics EXPRESS

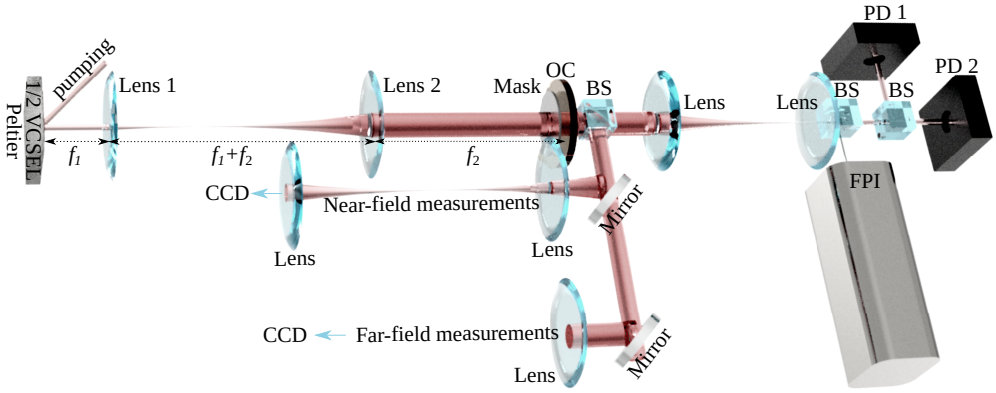

Fig. 1. Experimental setup. Lenses 1,2 form intracavity telescope (f_1 = 5 cm, f_2 = 20 cm). The metal mask placed at self-imaging position forms the laser array. Near-field and far-field of the array are captured by CCD cameras (u-eye UI-3240 NIR). Fabry-Perot interferometer (FPI) – FPI100 (FSP – 1 GHz, finesse - 280) is used for the spectral measurements. Noise measurements are performed with amplified photodiodes PDA015C/M (380 MHz bandwidth, 180 μm^2) with signal amplifiers ZFL-1000LN+ Low Noise Amplifier (0.1-1000 MHz, 20 dB gain).

provide a magnification of 4 in the 50-cm long cavity. The positions of lens 1 and of the output coupler are slightly adjusted with respect to strict geometric degeneracy in order to compensate for the thermal lens in the structure, as confirmed by an *ABCD* matrix analysis [49]. The setup allows one to capture the near-field, far-field, optical spectrum, and intensity signals simultaneously with the time synchronization accuracy of electronic devices. The laser array is created using a metal mask placed very close to the output coupler. It consists of circular holes of diameter σ = 200 μm with an edge-to-edge separation a = 50 μm. The near-field and far-field images of the laser array emission are captured by a CCD camera (u-eye UI-3240 NIR, exposition time 9μs). A Fabry-Perot interferometer (1 GHz free spectral range, finesse = 290) is used for spectral diagnostics. Intensity noise measurements are performed with a series of preamplified photodiodes PD1, PD2 (Thorlabs PDA015C/M: bandwidth 380 MHz, sensor area 180 μm^2) followed by low noise signal amplifiers (Mini-circuits ZFL-1000LN+: bandwidth 1-1000 MHz, gain 20 dB).

2.2. Calculation of the field overlap of adjacent lasers

Phase-locking of the lasers is achieved using injection locking from each laser to its neighbours thanks to diffraction from the mask. Diffracted light of each laser creates a coupling channel with its neighbors after reflection on the output coupler. In this case, the coupling strength is proportional to the field overlap between the two considered modes [32,50]. To calculate this overlap, we consider as shown in Fig. 2(a) a uniform constant field of amplitude E_0 for one of the lasers at the mask surface and propagate it over one round-trip to the output coupler and back to the mask using the following Huygens-Fresnel equation:

$$E^{1}\rho^{0o} = \frac{2\pi}{B\lambda}E_0 \int_0^{\sigma\cdot 2} \rho \exp\left[-i\frac{\pi}{B\lambda}{}^{1}A\rho^2 + D\rho^{02o}{}^{o}\right] J_0\left(\frac{2\pi}{B\lambda}\rho\rho^{0}\right) d\rho\,, \tag{1}$$

where the *ABCD* matrix describes propagation from the mask to the mirror and back, σ is the hole diameter, and ρ and ρ^0 are the radial coordinates for the input and output fields, respectively, described in cylindrical coordinates. Since the output coupler is flat, the matrix elements are simply $A = D = 1$, $C = 0$, and $B = 2l$, where l is the distance between the mask and the mirror.

Optics EXPRESS

It is worth noticing that a similar result would be obtained by considering propagation of the field in the opposite part of the cavity, i. e. from the mask, through the lenses to the gain chip and back to the mask, because the cavity degeneracy ensures that the *ABCD* matrix in this case would only differ by the sign of B.

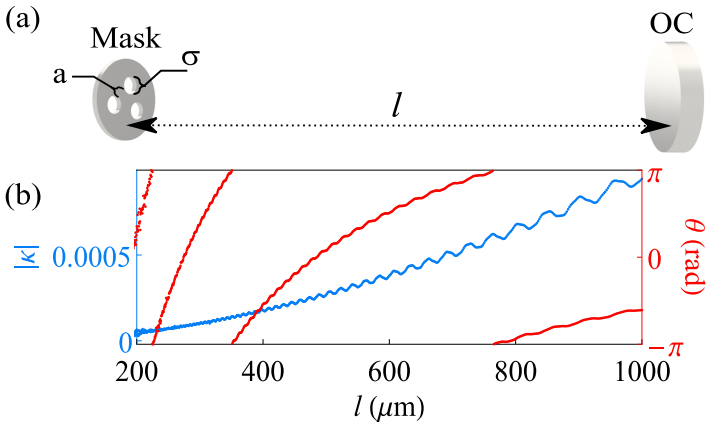

Fig. 2. Evolution of the mode overlap coefficient κ versus propagation distance l between the mask and OC (a). (b,c) Absolute value (blue) and argument (red) of κ, calculated with Eqs. (1,2) for l much shorter than the Talbot distance.

After propagation using Eq. (1), the fraction of complex field injected in the neighboring laser is obtained using the following expression:

$$\kappa = \frac{4}{\pi\sigma^2 E_0} \int_0^{2\pi} d\phi_2 \int_0^{\sigma\cdot 2} \rho^{00} E \left(q \_\_\_\_\_ \right) d\rho^{00}, \qquad (2)$$

where $c = \sigma + a$, with a the distance between the edges of the two neighbor holes (see Fig. 2(a)).

Figure 2 shows the evolution of the complex overlap coefficient κ calculated according to Eqs. (1) and (2) with the propagation distance l between the mask and the OC. This calculation is performed with the parameters of the experiment. The important thing to notice here is that κ is complex, with an argument θ evolving very quickly with l. Of course, we are here in the regime where l is very small compared to the Talbot distance $z_T = 2\sigma + a \cdot \lambda = 62$ mm, explaining why $|\kappa| \ll 1$.

The main conclusion of this section is that the phase-locking analysis that will be performed in section 3. requires to consider complex coupling coefficients.

2.3. Laser array phase-locking

The coupling calculated in the preceding subsection permits to control the phase-locking of the laser array, as is now going to be evidenced. Figure 3 represents near-field (NF) and far-field (FF) images of the VECSEL output in different conditions: (a) without any mask, (b,c) with a mask consisting of two holes, and (d, e) with a mask consisting of three holes in a triangular geometry. In all cases, the diameters of the holes are equal to $\sigma = 200\ \mu$m with an edge-to-edge separation $a = 50\ \mu$m. With such hole diameter, and with the low VECSEL gain and the losses introduced by the mask and the intracavity lenses, we could obtain only a maximum number of three lasers in the array. Of course, increasing the number of lasers would be highly desirable, provided we can reduce the thermal effects in the gain structure.

As predicted in the preceding subsection, the coupling between the lasers can be changed by translating the mask along the laser axis. This permits to change from an unlocked (Figs. 3(b,d)) to

Optics EXPRESS

Fig. 3. Near-field (NF) and far-field (FF) images of the laser emission. (a) No mask, (b) two unlocked lasers, (c) two phase-locked lasers, (d) three unlocked lasers, (e) three phase-locked lasers.

a locked (Figs. 3(c,e)) regime, as can be seen from the far-field patterns. To obtain phase-locking, the distance between the mask and the output coupler is of the order of 500 μm.

Throughout this paper, the laser array typically operates around $r = 1.1$ to $r = 1.2$ times above the threshold. The output power ranges between 0.32 and 3.12 mW, depending on the number of lasers in the array, the mask position, etc. Without the mask, the VECSEL has less losses and its output power is measured to be 53 mW, which corresponds to $r = 1.79$.

It is worth mentioning that in all cases the independence of the different lasers of the array can be checked by blocking each of them individually without affecting the powers of the other ones. By trying different masks, we could also notice that the number of spatial modes sustained by each laser and the laser array spectrum significantly depend on the diameter of the holes. Each hole corresponds to a single nearly Gaussian fundamental mode only when the hole diameter σ is no larger than 200 μm. In the perfectly degenerate cavity [51], the frequency detuning between the different lasers is supposed to be close to 0. But in practice the intracavity aberrations create some spurious detuning between the lasers. However, when the lasers are locked, they share the same frequency and operate in a single-frequency regime. This is evidenced by the optical spectrum shown in Fig. 4. The phase-locking of the laser array makes it remarkably robust: the laser single-frequency operation remains stable without any mode hop for several seconds in a standard laboratory environment. On the contrary, in the case where the laser array is unlocked, the laser spectrum is more unstable. This single-frequency operation will allow us in the following to establish a simple analytical model to describe the laser evolution. Moreover, it simplifies the understanding of the origin of laser noise by excluding mode beating and other effects related to multimode operation.

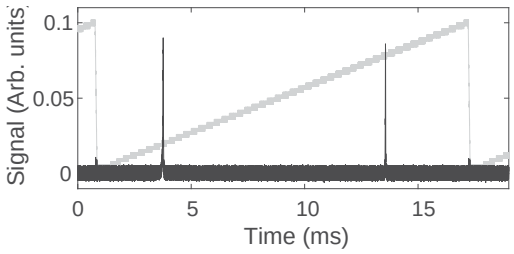

Fig. 4. Black line: optical spectrum obtained from the FPI for the array of two phase-locked lasers. Gray line: scan voltage of ramp applied to FPI. The free spectral range of the FPI is 1 GHz.

2.4. Noise of the laser array

The measurements of the relative intensity noise (RIN) spectrum of one of the lasers in the array of two lasers are reproduced in Fig. 5. The laser whose intensity noise is measured is the one in

Optics EXPRESS

the left of Figs. 3(b,c). In each case, the RIN spectrum of the other laser is very similar. Figure 5 compares the laser RIN when the two lasers are locked (blue line) and unlocked (red line). Apart from a difference in noise levels, which can be attributed to several reasons, such as a variation of the laser losses and power between the two cases, no significant difference appears between the two situations. We also checked that the same kind of RIN spectrum is obtained for an array of three lasers. In all cases, these spectra are typical of a class-A laser with a photon lifetime of the order of 30 ns, much longer than the carrier lifetime in the gain structure (a few ns). When one compares the laser RIN spectrum with the pump RIN spectrum (black line in Fig. 5), the filtering effect of the cavity above a 3 dB cut-off frequency of the order of 500 kHz is clearly visible.

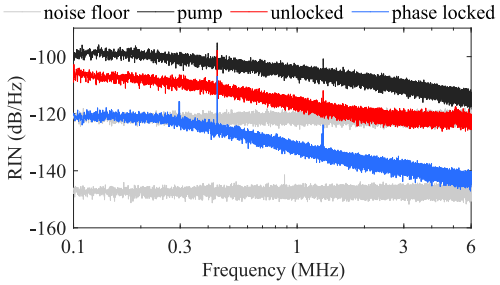

Fig. 5. Experimental RIN spectra of one of the lasers in the array of two lasers, while phase-locked (blue, laser output power of the order of 2 mW) and unlocked (red, laser output power of the order of 0.4 mW). Grey curve: noise floor. Black curve: pump laser RIN. Thin peaks originate from some spurious modulations of the laser power.

The difference between the RIN levels of the locked and unlocked laser arrays in Fig. 5 is due to the presence of extra losses in the unlocked case. Indeed, we observe experimentally that it is very easy to obtain phase-locking of the array as soon as the mask is introduced inside the cavity and creates a small coupling. The unlocked behavior of the laser array can only be obtained by slightly translating the mask inside the cavity, thus creating extra losses and decreasing the laser power.

Much more information on the laser array behavior can be gained by measuring the spectrum of the correlations between the intensity noises of the different lasers of the array. Figure 6 shows a few examples of such measurements. Figures 6(a) and 6(c) correspond to the amplitude of the normalized correlation spectrum between the intensity noises of two of the lasers in the array, while Figs. 6(b) and 6(c) display the phase of this correlation. In each plot, the blue (red) curve corresponds to the situation where the lasers of the array are phase-locked (unlocked). Figures 6(a,b) correspond to an array of two lasers while Figs. 6(c,d) was obtained for an array of three lasers.

Comparison of the two cases in this figure shows a dramatic difference between phase-locked and independent lasers. Indeed, while the correlation between the intensity noises between the lasers cannot be distinguished from noise when the lasers are unlocked (see the red curves in Figs. 6(a) and 6(c), these intensity fluctuations become almost completely correlated when the array is phase-locked (blue curves). This illustrates, by a measurement different from the one of Figs. 3 and 4, the fact that the lasers behave like completely independent oscillators when they are unlocked and that the laser array behaves like a single super-laser in a single supermode when the lasers are phase-locked. In the next section, we build a model to describe this abrupt change of behavior theoretically.

Optics EXPRESS

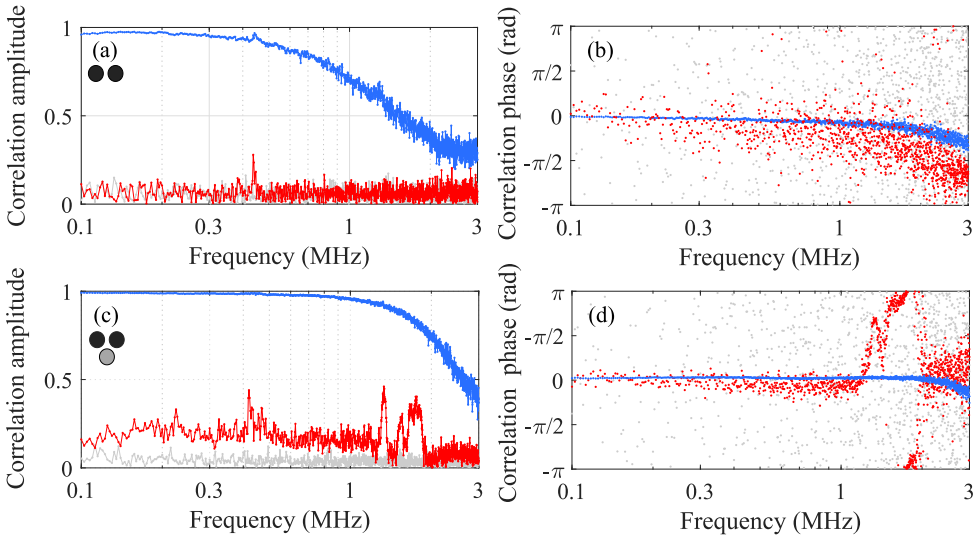

Fig. 6. Measured correlation spectra between the intensity fluctuations of two lasers in the array. (a,c) Amplitude and (b,d) phase of the correlation. Blue curves: phase-locked laser array, red curves: unlocked laser array; light gray curves: noise floor. (a,b) array of two lasers, (c,d) array of three lasers.

3. Analytical model

The model used to describe the intensity and phase noise of the lasers is based on a system of rate equations. In the following we present how the model is established in the simplest case of an array of two lasers coupled via diffraction on the intracavity mask. For simplicity, we suppose here that the two lasers are perfectly symmetric (same losses, same pumping rate). For the sake of conciseness, we do not give here the more general version of the model, which describes the behavior of larger laser arrays. But some results derived from this general model will be shown below.

3.1. Rate equations

We are interested in the influence of the pump noise on the laser array dynamics and noise characteristics. This noise is introduced as a fluctuation $\delta r_i {}^1t^0$ in the pumping rate $r + \delta r_i {}^1t^0$ of the laser i in the array, where r is the average pumping rate common to all the lasers. All other sources of noise such as spontaneous emission, vacuum fluctuations entering the resonator, etc, have a negligible effect in our experiments. Thermal noise is also neglected, since it was shown to have a significant influence on the laser phase noise only and not on the intensity noise [21–25].

The nanosecond carrier lifetime, much shorter than the photon lifetime in the cavity, lets us adiabatically eliminate the population inversion from the laser equations. Therefore, the

Optics EXPRESS

dynamics of the laser array is governed by the following rate equations (RS):

$$\begin{aligned}
\frac{\partial A_1}{\partial t} &= -\frac{A_1}{2\tau}\left(1-\frac{r+\delta r_1}{1+A_1^2\bullet F_{\mathrm{sat}}}\right)+\frac{|\eta|}{\tau}\cos(\psi+\theta)A_2,\\
\frac{\partial A_2}{\partial t} &= -\frac{A_2}{2\tau}\left(1-\frac{r+\delta r_2}{1+A_2^2\bullet F_{\mathrm{sat}}}\right)+\frac{|\eta|}{\tau}\cos(\psi-\theta)A_1,\\
\frac{\partial \psi}{\partial t} &= \frac{\alpha}{2\tau}\left(\frac{r+\delta r_2}{1+A_2^2\bullet F_{\mathrm{sat}}}-\frac{r+\delta r_1}{1+A_1^2\bullet F_{\mathrm{sat}}}\right)\\
&\quad -\frac{|\eta|}{\tau}\left(\frac{A_2}{A_1}\sin(\psi+\theta)+\frac{A_1}{A_2}\sin(\psi-\theta)\right)+\Delta,
\end{aligned} \tag{3}$$

where A_1 and A_2 are the amplitudes of the two laser fields, normalized in such a way that their squares correspond to the respective photon numbers. The third variable ψ is the phase difference between the lasers, F_{sat} the saturation photon number. The complex coupling introduced by diffraction from the mask corresponds to the term $\eta\, e^{i\theta}$. We assume, that the coupling coefficient η is proportional to the mode overlap coefficient κ of Fig. 2. The fact that the value of $|\eta|$ introduced in the simulations to reproduce the experimental results is systematically larger than the calculated value of $|\kappa|$ is attributed to the imperfections of the experimental setup (rough edges of holes in the mask, non-flat top profile etc.). The present model is applicable to any laser array geometry and any mask position by adjusting the value of η.

Phase-locking of two lasers requires the absolute value of the coupling strength to exceed the critical value $|\eta_{\mathrm{cr}}| = \frac{\tau}{2}$ [52]. This formula is valid in the case where the lasers have identical parameters in terms of pumping rate, losses, cavity lifetime, and real-valued η. In the case where η is no longer real but complex, i.e., $\eta = |\eta| e^{i\theta}$, phase-locking occurs above the critical value its critical value gives $|\eta| \geq |\eta_{\mathrm{cr}}| = \tau\bullet 2\cos\theta$.

The fluctuations of the lasers around their steady-state solutions are obtained by linearizing Eqs. (3) around the steady state. Following Ref. [24], the three variables are written in vector form as $\mathbf{A} = \{A_{1,\mathrm{st}}, A_{2,\mathrm{st}}, \psi_{21,\mathrm{st}}\} + \delta\mathbf{A}$, where the vector $\delta\mathbf{A} = \{\delta A_1, \delta A_2, \delta\psi\}$ contains the fluctuations around the steady-state values $\{A_{1,\mathrm{st}}, A_{2,\mathrm{st}}, \psi_{\mathrm{st}}\}$. The pump fluctuations around the average value r_0 are written as a vector $\delta\mathbf{r} = \{\delta r_1, \delta r_2\}$. Then the RS system of Eqs. (3) can be formally written as:

$$\dot{\mathbf{A}}(t) = RS(\mathbf{A}, \mathbf{r}(t)) = RS(\mathbf{A}_{\mathrm{st}} + \delta\mathbf{A}, \mathbf{r}_0 + \delta\mathbf{r}) \tag{4}$$

Linearization consists in expanding the right-hand side up to the first order in $\delta\mathbf{r}$ and $\delta\mathbf{A}$, leading to:

$$\delta\dot{\mathbf{A}}(t) = \underbrace{RS(\mathbf{r}_0, \mathbf{A}_{\mathrm{st}})}_{=0} + \frac{\partial RS(\mathbf{r}, \mathbf{A})}{\partial \mathbf{A}}\Big|_{r_0, A_{\mathrm{st}}}\delta\mathbf{A} + \frac{\partial RS(\mathbf{r}, \mathbf{A})}{\partial \mathbf{r}}\Big|_{r_0, A_{\mathrm{st}}}\delta\mathbf{r}\,. \tag{5}$$

The steady-state solution for the system of two lasers, in the case where they are phase-locked, depends on the frequency detuning between the lasers. For small values of , the steady-state phase difference is:

$$\psi_{\mathrm{st}} = \begin{cases} \pi - \arcsin\frac{\eta_{\mathrm{cr}}}{\eta} + 2\pi n\,, & \text{if } \eta<0\,,\\ \arcsin\frac{\eta_{\mathrm{cr}}}{\eta} + 2\pi n\,, & \text{if } \eta>0\,, \end{cases} \tag{6}$$

where n 2 Z. In the following, since the experiment doesn't provide us any mean to measure the value of , we will simply take = 0. In this case the steady-state solution becomes:

$$\psi_{\mathrm{st}} = \pi\,, \tag{7}$$

Optics EXPRESS

$$A_{1,\mathrm{st}} = A_{2,\mathrm{st}} = \sqrt{\frac{r}{F_{\mathrm{sat}}\dfrac{r}{1-2\eta\cos\theta}-1}}\,. \tag{8}$$

Taking the Fourier transform of Eq. (5) leads to the following algebraic expression:

$$\delta\tilde{A}(\omega) = \left[i\omega - \frac{\partial RS(r,A)}{\partial A}\Big|_{r_0,A_{\mathrm{st}}}\right]^{-1} \frac{\partial RS(r,A)}{\partial r}\Big|_{r_0,A_{\mathrm{st}}}\delta\tilde{r}(\omega) \tag{9}$$

where the tilde denotes the Fourier transformed variables. The intensity fluctuations in the frequency domain are then obtained as follows:

$$\delta\tilde{I}(\omega) = 2A_{\mathrm{st}}\left[i\omega - \frac{\partial RS(r,A)}{\partial A}\Big|_{r_0,A_{\mathrm{st}}}\right]^{-1} \frac{\partial RS(r,A)}{\partial r}\Big|_{r_0,A_{\mathrm{st}}}\delta\tilde{r}(\omega)\,, \tag{10}$$

from which one can deduce the RIN spectra of the two lasers and the cross-correlation spectrum between their amplitude fluctuations, in the following way:

$$\mathrm{CC}(\delta I_1, \delta I_2) = \frac{\mathrm{Cov}(\delta A_1, \delta A_2)}{\sqrt{\mathrm{Var}(\delta A_1)\mathrm{Var}(\delta A_2)}}\,, \tag{11}$$

in which Var holds for the variance and Cov for the covariance.

Some RIN spectra numerically calculated from Eq. (3) with parameter values typical of our experimental setup are shown in Fig. 7. This figure contains three RIN spectra, all obtained with the same parameter values, except for the value of the coupling coefficient η, which is 0 for the red curve, real for the light green curve, and complex for the dark blue curve. The two lasers are unlocked in the former case and phase-locked in the two latter cases. One notices that these RIN spectra exhibit the typical first-order filter shape of class-A laser, as observed experimentally in Fig. 5. The difference between the phase-locked and unlocked situations consists of a small change in the noise level and the noise cutoff frequency. The small change in cutoff frequency can be easily understood from the analytical expressions above. Indeed, Eq. (5) corresponds to a linearization around a steady-state solution, whose expression depends on the coupling coefficient according to Eq. (6).

The difference between the three situations is much more striking when one considers the correlations between the noises of the two lasers, as shown by the simulations results reproduced in Fig. 8. A very good agreement is obtained with the experimental results of Fig. 6: the correlation is almost zero when the two lasers are unlocked and much larger when the two lasers are locked with $\alpha = 6$, which is a typical value for the gain chip we used in our experiments. Moreover, the phase of this correlation is zero, showing that the correlated parts of the intensity noises of the two modes are in phase, as observed experimentally.

Concerning the analytical model based on linearization of the laser behavior around steady-state, some typical RIN spectra obtained from Eq. (10) are shown in Fig. 9, but will be more thoroughly discussed in the next subsection.

3.2. Role of the Henry α-factor

The comparison of the light green and blue curves in Fig. 8(a) illustrates the role of the phase of the coupling coefficient η on the amplitude noise correlation. The question that we wish to address in the present section is to know whether this sensitivity to the coupling phase is linked with the large value of Henry's α factor in our VECSEL active quantum wells.

To this aim, we simulated the noise behavior of an array of two lasers for different values of α and for both real and complex values of the coupling coefficient η. The results are shown in Fig. 9. In each of the plots of Fig. 9, the dashed lines correspond to cases where η is real ($\theta = 0$)

Optics EXPRESS

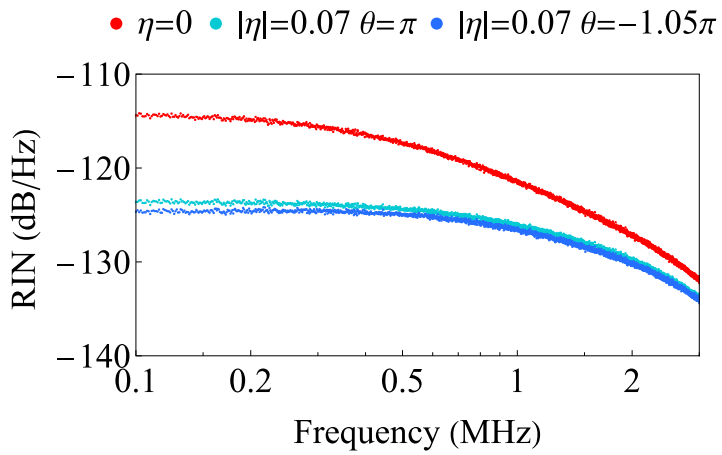

Fig. 7. Theoretical laser RIN spectra for an array of two lasers. The two curves correspond to two different coupling coefficients between neighboring lasers. The spectra were calculated with $\alpha = 6$, $r = 1.1$, $\eta = 0$ and 0.07, $\tau = 30$ ns, and •$2\pi = 0$. The pump noise spectra are taken to be white and fully uncorrelated in the considered frequency range with a RIN = −135 dB. The presented data corresponds to the averaging of over 1000 noise spectra.

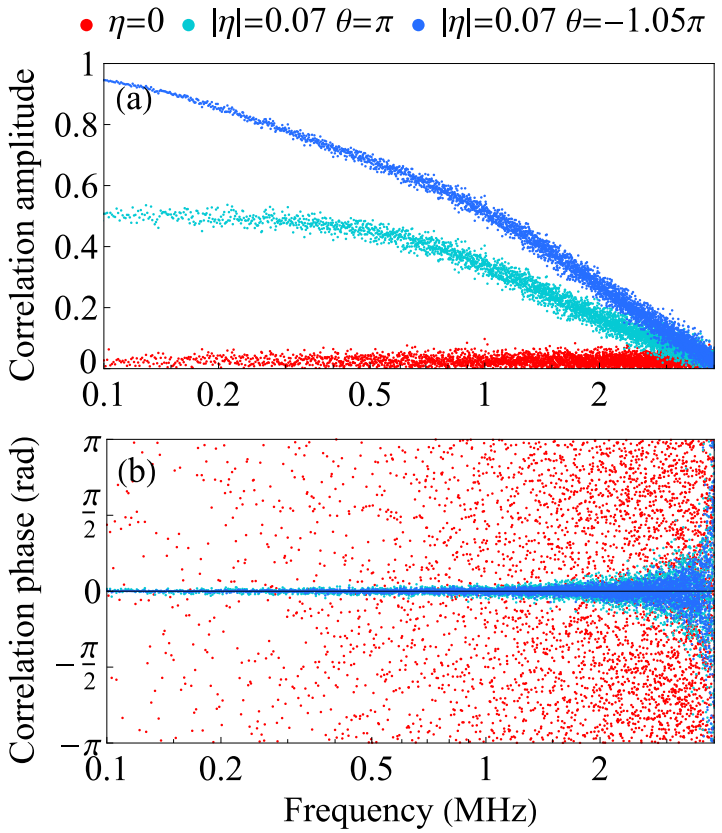

Fig. 8. Laser noise amplitude and phase correlation spectrum between the intensity noises of the two lasers obtained with the numerical model. The data were calculated with the same parameters as Fig. 7. The presented data corresponds to the averaging of over 1000 noise spectra.

Optics EXPRESS

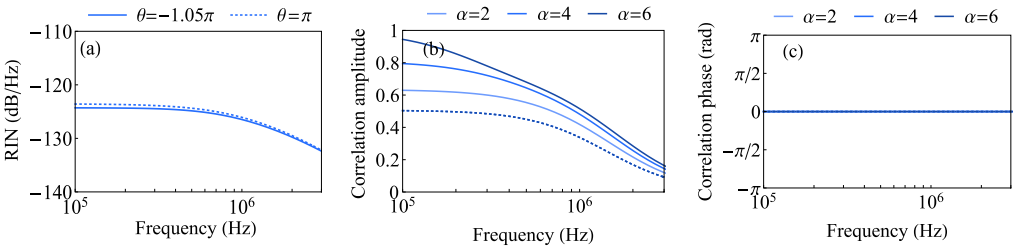

Fig. 9. (a) RIN spectrum of one of the lasers and (b) amplitude and (c) phase of the correlation spectrum between the intensity noises of the two lasers obtained with the analytical model. The data were calculated for $r = 1.1$, $\eta = 0.07$, $\tau = 30$ ns, and $\bullet 2\pi = 0$. The blue data set ($\alpha = 6$) should be compared with the blue curve in Fig. 7.

while full lines correspond to a complex value for η, with an argument $\theta = -1.05\,\pi$. In these figures, the curves of different colors correspond to different values of α, ranging from 3 to 9.

First of all, Fig. 9(a) shows that the RIN spectrum of the lasers hardly depends on α and θ. However, the situation is different when one looks at the correlation amplitude between the intensity fluctuations of the two modes, as shown in Fig. 9(b). Indeed, in this figure, the fact that the three dashed lines are perfectly superimposed shows that α has no impact on the correlation amplitude as long as $\theta = 0$, i.e., as long as the coupling coefficient η is real. On the contrary, the three full lines in Fig. 9(b) show that as soon as η is complex, the correlation amplitude strongly increases with α. Besides, Fig. 9(c) shows that in all cases the phase of the correlation remains close to 0, at least in the frequency range where the correlation amplitude is significant.

The physical explanation behind this α-dependence of the correlation amplitude when η is complex lies in the fact that a complex coupling coefficient breaks the system symmetry, while the α factor enhances any system asymmetry. The same kind of phenomenon can be shown to occur if there is an unbalance between some parameters of the two lasers, such as for example the pump fluctuations δr_i.

4. Conclusion

In conclusion, we have theoretically and experimentally studied the phase-locking and noise behavior of an array of lasers based on a degenerate cavity VECSEL operating as a class-A laser. In this system, the lasers are defined by a mask, which is also responsible, through diffraction, for the coupling between the lasers. The experiments and the model show that depending on the amount of coupling, the lasers in the array can be phase-locked or not. Moreover, we have performed measurements of the intensity noises of the lasers and of the correlations between the noises of different lasers. These measurements show that the correlation amplitude dramatically depends on whether the lasers in the array are phase-locked or not. A very small correlation between the laser noises is found when they are unlocked, while they get almost fully correlated once they get phase-locked. These observations are fully reproduced by our rate equation model that includes the diffraction coupling between the lasers, the pump noise, and the Henry phase-amplitude coupling coefficient typical of semiconductor active media. This model shows that two parameters play an important role in the laser noise dynamics. First, the fact that the distance between the mask and the cavity mirror is small leads to a complex value of coupling between the lasers. This has been shown to lead to a modification of the correlations between the intensity noises of the lasers. Second, the Henry factor is also shown to play an important role: as soon as the coupling coefficient is complex, it also contributes to increase the correlation between the laser intensity noises. Moreover, the combination of a complex coupling coefficient

Optics EXPRESS

and a large Henry factor should also lead to an amplification of the effect of asymmetries in the parameters of the different lasers in the array, such as their gain, losses, etc.

Future work includes the increase of the number of lasers in the array. Among other issues, this requires the reduction of the thermal lensing effect in the gain chip [47].

Funding. Science and Engineering Research Board (SIR/2022/00019); RENATECH; PAUSE.

Disclosures. The authors declare no conflicts of interest.

Data availability. Data underlying the results presented in this paper are not publicly available at this time but may be obtained from the authors upon reasonable request.

References

1. V. Pal, C. Trandonsky, R. Chriki, G. Barach, A. A. Friesem, and N. Davidson, "Phase locking of even and odd number of lasers on a ring geometry: Effects of topological-charge," Opt. Express 23(10), 13041–13050 (2015).
2. V. Pal, C. Tradonsky, R. Chriki, A. A. Friesem, and N. Davidson, "Observing Dissipative Topological Defects with Coupled Lasers," Phys. Rev. Lett. 119(1), 013902 (2017).
3. V. Dev and V. Pal, "Divergence and self-healing of a discrete vortex formed by phase-locked lasers," J. Opt. Soc. Am. B 38(12), 3683 (2021).
4. K. Takata, S. Utsunomiya, and Y. Yamamoto, "Transient time of an Ising machine based on injection-locked laser network," New J. Phys. 14(1), 013052 (2012).
5. K. Takata and Y. Yamamoto, "Data search by a coherent Ising machine based on an injection-locked laser network with gradual pumping or coupling," Phys. Rev. A 89(3), 032319 (2014).
6. K. Takata, A. Marandi, R. Hamerly, Y. Haribara, D. Maruo, S. Tamate, H. Sakaguchi, S. Utsunomiya, and Y. Yamamoto, "A 16-bit coherent Ising machine for one-dimensional ring and cubic graph problems," Sci. Rep. 6(1), 34089 (2016).
7. M. Nixon, E. Ronen, A. A. Friesem, and N. Davidson, "Observing geometric frustration with thousands of coupled lasers," Phys. Rev. Lett. 110(18), 184102 (2013).
8. C. Tradonsky, I. Gershenzon, V. Pal, R. Chriki, A. A. Friesem, O. Raz, and N. Davidson, "Rapid laser solver for the phase retrieval problem," Sci. Adv. 5(10), eaax4530 (2019).
9. V. Pal, S. Mahler, C. Tradonsky, A. Friesem, and N. Davidson, "Rapid fair sampling of the XY spin Hamiltonian with a laser simulator," Phys. Rev. Res. 2(3), 033008 (2020).
10. D. Saxena, A. Arnaudon, O. Cipolato, M. Gaio, A. Quentel, S. Yaliraki, D. Pisignano, A. Camposeo, M. Barahona, and R. Sapienza, "Sensitivity and spectral control of network lasers," Nat. Commun. 13(1), 6493 (2022).
11. M.-A. Miri and V. Menon, "Neural computing with coherent laser networks," Nanophotonics 12(5), 883–892 (2023).
12. K. Grobe, M. H. Eiselt, S. Pachnicke, and J.-P. Elbers, "Access networks based on tunable lasers," J. Lightwave Technol. 32(16), 2815–2823 (2014).
13. E. K. Lau, X. Zhao, H.-K. Sung, D. Parekh, C. Chang-Hasnain, and M. C. Wu, "Strong optical injection-locked semiconductor lasers demonstrating > 100-GHz resonance frequencies and 80-GHz intrinsic bandwidths," Opt. Express 16(9), 6609–6618 (2008).
14. T. Alexoudi, G. Kanellos, and N. Pleros, "Optical RAM and integrated optical memories: a survey," Light: Sci. Appl. 9(1), 91 (2020).
15. M. Gu, X. Li, and Y. Cao, "Optical storage arrays: a perspective for future big data storage," Light: Sci. Appl. 3(5), e177 (2014).
16. S. Mitsugi, K. Suzuki, K. Kurihara, and T. Horibe, "Microoptical two-dimensional devices for the optical memory head of an ultrahigh data transfer rate and density sytem using a vertical cavity surface emitting laser (VCSEL) array," Jpn. J. Appl. Phys. 41(Part 1, No. 7B), 4835–4840 (2002).
17. C.-H. Chen, S. Matsuo, K. Nozaki, A. Shinya, T. Sato, Y. Kawaguchi, H. Sumikura, and M. Notomi, "All-optical memory based on injection-locking bistability in photonic crystal lasers," Opt. Express 19(4), 3387–3395 (2011).
18. L. Anderegg, L. Cheuk, Y. Bao, S. Burchesky, W. Ketterle, K.-K. Ni, and J. Doyle, "An optical tweezer array of ultracold molecules," Science 365(6458), 1156–1158 (2019).
19. S. C. Burd, D. T. C. Allcock, T. Leinonen, J. P. Penttinen, D. H. Slichter, R. Srinivas, A. C. Wilson, R. Jördens, M. Guina, D. Leibfried, and D. J. Wineland, "VECSEL systems for the generation and manipulation of trapped magnesium ions," Optica 3(12), 1294–1299 (2016).
20. K. Petermann, *Laser Diode Modulation and Noise* (Springer, 1991).
21. H. Liu, G. Gredat, G. Baili, F. Gutty, F. Goldfarb, I. Sagnes, and F. Bretenaker, "Noise investigation of a dual-frequency VECSEL for application to cesium clocks," J. Lightwave Technol. 36(18), 3882–3891 (2018).
22. G. Gredat, D. Chatterjee, G. Baili, F. Gutty, I. Sagnes, F. Goldfarb, F. Bretenaker, and H. Liu, "Fully–correlated multi–mode pumping for low–noise dual–frequency VECSELs," Opt. Express 26(20), 26217–26226 (2018).
23. G. Gredat, H. Liu, J. Cotxet, F. Tricot, G. Baili, F. Gutty, F. Goldfarb, I. Sagnes, and F. Bretenaker, "Optimization of laser dynamics for active stabilization of DF-VECSELs dedicated to cesium CPT clocks," J. Opt. Soc. Am. B 37(4), 1196 (2020).
24. S. S. De, V. Pal, A. E. Amili, G. Pillet, G. Baili, M. Alouini, I. Sagnes, R. Ghosh, and F. Bretenaker, "Intensity noise correlations in a two-frequency VECSEL," Opt. Express 21(3), 2538–2550 (2013).

Optics EXPRESS

25. S. De, G. Loas, A. E. Amili, M. Alouini, and F. Bretenaker, "Theoretical and experimental analysis of intensity noise correlations in an optically pumped, dual-frequency Nd:YAG laser," J. Opt. Soc. Am. B 30(11), 2830 (2013).
26. N. Davidson, S. Mahler, A. Friesem, and A. Forbes, "Complex-light lasers," Opt. Photonics News 33(5), 26–33 (2022).
27. M. Fridman, M. Nixon, N. Davidson, and A. A. Friesem, "Passive phase locking of 25 fiber lasers," Opt. Lett. 35(9), 1434–1436 (2010).
28. M. Fridman, M. Nixon, E. Ronen, A. A. Friesem, and N. Davidson, "Phase locking of two coupled lasers with many longitudinal modes," Opt. Lett. 35(4), 526–528 (2010).
29. E. Kapon, J. Katz, and A. Yariv, "Supermode analysis of phase-locked arrays of semiconductor lasers," Opt. Lett. 9(4), 125–127 (1984).
30. H. G. Winful and S. S. Wang, "Stability of phase locking in coupled semiconductor laser arrays," Appl. Phys. Lett. 53(20), 1894–1896 (1988).
31. F. X. D'Amato, E. T. Siebert, and C. Roychoudhuri, "Coherent operation of an array of diode lasers using a spatial filter in a Talbot cavity," Appl. Phys. Lett. 55(9), 816–818 (1989).
32. A. F. Glova, "Phase locking of optically coupled lasers," Quantum Electron. 33(4), 283–306 (2003).
33. A. A. Friesem, B. Redding, H. Cao, M. Nixon, and N. Davidson, "Efficient method for controlling the spatial coherence of a laser," Opt. Lett. 38(19), 3858–3861 (2013).
34. F. Arecchi, G. Lippi, G. Puccioni, and J. Tredicce, "Deterministic chaos in laser with injected signal," Opt. Commun. 51(5), 308–314 (1984).
35. G. Baili, M. Alouini, D. Dolfi, and F. Bretenaker, "Shot-noise-limited operation of a monomode high-cavity-finesse semiconductor laser for microwave photonics applications," Opt Lett (2007).
36. G. Baili, F. Bretenaker, M. Alouini, L. Morvan, D. Dolfi, and I. Sagnes, "Experimental investigation and analytical modeling of excess intensity noise in semiconductor class-A lasers," J. Lightwave Technol. 26(8), 952–961 (2008).
37. G. Baili, L. Morvan, G. Pillet, S. Bouchoule, Z. Zhao, J.-L. Oudar, L. Ménager, S. Formont, F. V. Dijk, M. Faugeron, M. Alouini, F. Bretenaker, and D. Dolfi, "Ultralow noise and high-power vecsel for high dynamic range and broadband RF/optical links," J. Lightwave Technol. 32(20), 3489–3494 (2014).
38. S. Knitter, C. Liu, B. Redding, M. K. Khokha, M. A. Choma, and H. Cao, "Coherence switching of a degenerate VECSEL for multimodality imaging," Optica 3(4), 403–406 (2016).
39. Y. Bouchereau, S. Karuseichyk, R. Guitter, V. Pal, and F. Bretenaker, "Effect of linewidth enhancement factor on the generation of optical vortices in a class-A degenerate cavity semiconductor laser," Opt. Express 30(9), 15648–15658 (2022).
40. A. Zilkie, J. Meier, M. Mojahedi, A. S. Helmy, P. J. Poole, P. Barrios, D. Poitras, T. J. Rotter, C. Yang, A. Stintz, K. Malloy, P. W. E. Smith, and J. S. Aitchison, "Time-resolved linewidth enhancement factors in quantum dot and higher-dimensional semiconductor amplifiers operating at 1.55 μm," J. Lightwave Technol. 26(11), 1498–1509 (2008).
41. A. Consoli, B. Bonilla, J. M. G. Tijero, and I. Esquivias, "Self-validating technique for the measurement of the linewidth enhancement factor in semiconductor lasers," Opt. Express 20(5), 4979–4987 (2012).
42. T. Fordell and A. M. Lindberg, "Experiments on the linewidth-enhancement factor of a vertical-cavity surface-emitting laser," IEEE J. Quantum Electron. 43(1), 6–15 (2007).
43. B. Sinquin and M. Romanelli, "Determination of the linewidth enhancement factor of semiconductor lasers by complete optical field reconstruction," Opt. Lett. 48(4), 863–866 (2023).
44. J. Stohs, D. Bossert, D. Gallant, and S. Brueck, "Gain, refractive index change, and linewidth enhancement factor in broad-area GaAs and InGaAs quantum-well lasers," IEEE J. Quantum Electron. 37(11), 1449–1459 (2001).
45. A. Thorette, M. Romanelli, and M. Vallet, "Linewidth enhancement factor measurement based on FM-modulated optical injection: application to rare-earth-doped active medium," Opt. Lett. 42(8), 1480–1483 (2017).
46. A. A. Bartolo González, "Spatial organization of localized pulses in a self-imaging vertical external cavity surface emitting laser," Thesis, Université Côte d'Azur (2022).
47. M. Guina, A. Rantamäki, and A. Härkönen, "Optically pumped VECSELs: Review of technology and progress," J. Phys. D: Appl. Phys. 50(38), 383001 (2017).
48. A. Laurain, M. Myara, G. Beaudoin, I. Sagnes, and A. Garnache, "High power single–frequency continuously–tunable compact extended–cavity semiconductor laser," Opt. Express 17(12), 9503–9508 (2009).
49. A. Bartolo, N. Vigne, M. Marconi, G. Beaudoin, K. Pantzas, I. Sagnes, G. Huyet, F. Maucher, S. V. Gurevich, J. Javaloyes, A. Garnache, and M. Giudici, "Temporal localized Turing patterns in mode-locked semiconductor lasers," Optica 9(12), 1386–1393 (2022).
50. D. Mehuys, W. Streifer, R. G. Waarts, and D. F. Welch, "Modal analysis of linear talbot-cavity semiconductor lasers," Opt. Lett. 16(11), 823–825 (1991).
51. S. Mahler, Y. Eliezer, H. Yilmaz, A. A. Friesem, N. Davidson, and H. Cao, "Fast laser speckle suppression with an intracavity diffuser," Nanophotonics 10(1), 129–136 (2020).
52. L. Fabiny, P. Colet, R. Roy, and D. Lenstra, "Coherence and phase dynamics of spatially coupled solid-state lasers," Phys. Rev. A 47(5), 4287–4296 (1993).